

BRAIN COMMUNICATIONS

Epileptic discharges initiate from brain areas with elevated accumulation of α -amino-3-hydroxy-5-methyl-4-isoxazole propionic acid receptors

Tomoyuki Miyazaki,^{1*} Yutaro Takayama,^{2*} Masaki Iwasaki,^{2*} Mai Hatano,¹ Waki Nakajima,¹ Naoki Ikegaya,³ Tetsuya Yamamoto,³ Shohei Tsuchimoto,⁴ Hiroki Kato⁵ and  Takuya Takahashi¹

* These authors contributed equally to this work.

Presurgical identification of the epileptogenic zone is a critical determinant of seizure control following surgical resection in epilepsy. Excitatory glutamate α -amino-3-hydroxy-5-methyl-4-isoxazole propionic acid receptor is a major component of neurotransmission. Although elevated α -amino-3-hydroxy-5-methyl-4-isoxazole propionic acid receptor levels are observed in surgically resected brain areas of patients with epilepsy, it remains unclear whether increased α -amino-3-hydroxy-5-methyl-4-isoxazole propionic acid receptor-mediated currents initiate epileptic discharges. We have recently developed the first PET tracer for α -amino-3-hydroxy-5-methyl-4-isoxazole propionic acid receptor, [¹¹C]K-2, to visualize and quantify the density of α -amino-3-hydroxy-5-methyl-4-isoxazole propionic acid receptors in living human brains. Here, we detected elevated [¹¹C]K-2 uptake in the epileptogenic temporal lobe of patients with mesial temporal lobe epilepsy. Brain areas with high [¹¹C]K-2 uptake are closely colocalized with the location of equivalent current dipoles estimated by magnetoencephalography or with seizure onset zones detected by intracranial electroencephalogram. These results suggest that epileptic discharges initiate from brain areas with increased α -amino-3-hydroxy-5-methyl-4-isoxazole propionic acid receptors, providing a biological basis for epileptic discharges and an additional non-invasive option to identify the epileptogenic zone in patients with mesial temporal lobe epilepsy.

- 1 Department of Physiology, Yokohama City University Graduate School of Medicine, Yokohama 236-0004, Japan
- 2 Department of Neurosurgery, National Center Hospital, National Center of Neurology and Psychiatry, Kodaira 187-8551, Japan
- 3 Department of Neurosurgery, Yokohama City University Graduate School of Medicine, Yokohama 236-0004, Japan
- 4 Division of System Neuroscience, National Institute for Physiological Sciences, Okazaki 444-8585, Japan
- 5 Department of Nuclear Medicine and Tracer Kinetics, Osaka University Graduate School of Medicine, Suita 565-0871, Japan

Correspondence to: Takuya Takahashi
Department of Physiology, Yokohama City University Graduate School of Medicine
Fukuura 3-9, Kanazawa-ku, Yokohama, 236-0004, Japan
E-mail: takahast@yokohama-cu.ac.jp

Keywords: AMPA receptor; positron emission tomography; magnetoencephalography; intracranial electroencephalogram; equivalent current dipole

Abbreviations: ECD = equivalent current dipole; FDG = ¹⁸F-fluorodeoxyglucose; FG = fusiform gyrus; FOV = field of view; HIP = hippocampus; IED = interictal epileptiform discharge; ITG = inferior temporal gyrus; LGA = Logan graphical analysis;

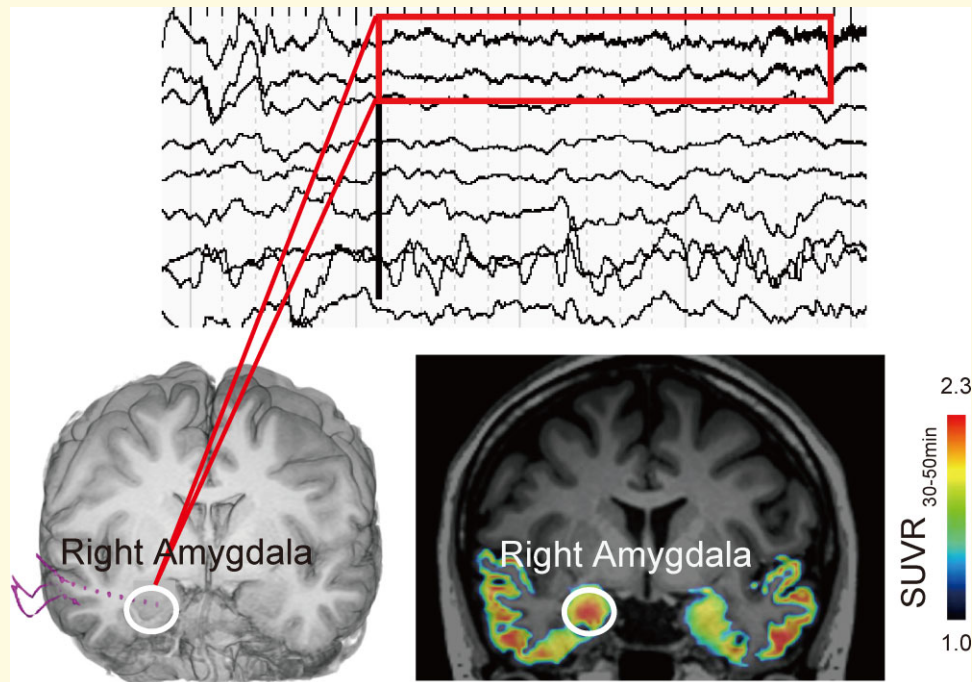
Received August 30, 2021. Revised November 11, 2021. Accepted February 3, 2022. Advance access publication February 7, 2022

© The Author(s) 2022. Published by Oxford University Press on behalf of the Guarantors of Brain.

This is an Open Access article distributed under the terms of the Creative Commons Attribution License (<https://creativecommons.org/licenses/by/4.0/>), which permits unrestricted reuse, distribution, and reproduction in any medium, provided the original work is properly cited.

MEG = magnetoencephalography; MNI = Montreal Neurological Institute; MTG = middle temporal gyrus; MTLE = mesial temporal lobe epilepsy; SOZ = seizure onset zone; SPM = statistical parametric mapping; SUVR = standardized uptake value ratio; VOI = volume of interest

Graphical Abstract



Introduction

Approximately 20–30% of patients with epilepsy are drug-resistant and surgical removal of the clinically suspected epileptogenic zone is often effective for seizure control in patients with drug-resistant epilepsy.¹ However, to improve surgical outcomes, there is a need for a diagnostic modality that can identify the entire epileptogenic zone directly.² The glutamate α -amino-3-hydroxy-5-methyl-4-isoxazole propionic acid receptor (AMPA) is a central mediator of neurotransmission in the brain.^{3–12} Surgically removed specimens from patients with epilepsy exhibit increased AMPARs.¹³ Furthermore, the administration of perampamil, a selective non-competitive AMPAR antagonist, reduces epileptic seizures.^{14,15} These results suggest that the elevation of AMPAR levels is related to epileptic activities. To visualize and quantify the density of AMPARs in living human brains, we recently developed the first PET tracer, [¹¹C]K-2.^{16–18} Further, we found that [¹¹C]K-2 represents the density of cell surface AMPARs.¹⁷ We detected elevated [¹¹C]K-2 uptake in brain areas that included clinically identified epileptogenic zone.¹⁶ However, it remains unclear whether brain areas with high AMPAR accumulation initiate epileptic discharges in living human brains. Magnetoencephalography (MEG) signals are derived from the net effect of postsynaptic ionic currents that flow in the dendrites of neurons under

synaptic transmission and are generated by a substantial population of neurons aligned in the same direction.^{19,20} Compared with EEG signals, MEG signals are less influenced by the difference in electrical conductivities between the CSF, skull and skin, as these tissues that surround the brain have constant magnetic permeability.²¹ Thus, MEG is a non-invasive modality that estimates the source of interictal epileptiform discharges (IEDs).²² Herein, IED was modelled using a single equivalent current dipole (ECD).²³ Therefore, MEG can approximate the localization of IEDs and help identify the irritative zones. Removal of the ECD area is known to be associated with postoperative seizure control in patients with epilepsy.^{24,25} Here, we characterized the irritative and seizure onset zones (SOZs) using [¹¹C]K-2 in combination with MEG or intracranial EEG (iEEG). We performed PET scans using [¹¹C]K-2 and MEG in five patients with mesial temporal lobe epilepsy (MTLE) who underwent surgical resections of the suspected epileptogenic zones that were identified by the non-invasive evaluations. We found that ECDs colocalized with brain areas of elevated [¹¹C]K-2 uptake in the surgically resected areas, compared with the contralateral hemisphere. Furthermore, we performed iEEG in one patient, in whom we detected higher [¹¹C]K-2 uptake in the SOZ than in other brain areas. Thus, we demonstrated that elevated AMPAR levels underlie the genesis of epileptic discharges.

Materials and methods

Human participants

Patients with epilepsy

The clinical trial to evaluate the efficacy of [¹¹C]K-2 in refractory epilepsy patients undergoing anterior temporal lobectomy (trial registry number UMIN00025090) was carried out to examine the efficacy of [¹¹C]K-2 in measuring the density of AMPA receptors in patients with epilepsy. Detailed information about the participants and the study design was previously reported by Miyazaki *et al.*¹⁶ In short, eight patients diagnosed with refractory MTLE based on a non-invasive assessment met the eligibility criteria and were registered. Five of the eight patients underwent MEG, and one underwent iEEG, all of whom provided data that were analysed in this study. Five patients (one male and four females) with drug-resistant MTLE underwent respective temporal surgery at the National Center Hospital, National Center of Neurology and Psychiatry, and had undergone at least 1 year of postoperative follow-up. The clinical characteristics of the patients are summarized in Table 1. The mean age at the PET examination of [¹¹C]K-2 was 39.8 years (range, 21–58 years). The mean duration from the diagnosis of epilepsy to the PET examination of [¹¹C]K-2 was 32.4 years (range, 8–51 years).

All five patients underwent presurgical comprehensive epilepsy evaluations that included medical interviews, neurological and neuropsychological examinations, long-term video-electroencephalography, MRI, ¹⁸F-fluorodeoxyglucose-PET (FDG-PET) and MEG. Epilepsy histories were obtained from the patients and their relatives, and the semiology of their habitual seizures was confirmed. The epilepsy diagnoses and classifications were established after comprehensive evaluations. The MRI evaluations revealed structural abnormalities in all patients, and four of the five had hippocampal sclerosis (Table 1). Abnormal hypometabolism on FDG-PET was also observed in all the patients.

Magnetoencephalography

MEG was recorded with simultaneous scalp-EEG for 40-min periods during awake and sleep conditions using a 1000 Hz sampling rate and band-pass filter between 0.03 and 330 Hz, with a whole-head system that consisted of 204 planar gradiometers (Elekta, Helsinki, Finland). The location of the dipole sources that best fit the measured magnetic fields was calculated using a single ECD model at the peak of each spike. We selected and presented ECDs that showed >90% goodness-of-fit value for the evaluation. The estimated ECDs were plotted on the co-registered [¹¹C]K-2 images using the PMOD Fusion tool v3.7 (PMOD Technologies). We qualitatively evaluated the locational relationship between the estimated ECDs and brain areas with high [¹¹C]K-2 uptake.

Table 1 Clinical characteristics

Case	Sex	Age at first seizure on [¹¹ C]K-2-PET (Y)	Age at AED surgery on [¹¹ C]K-2-PET (dose)	Seizure frequency	Seizure frequency	Location of scalp-EEG abnormality			Location of ECDs estimated by MEG (total number of ECDs)	Location of FDG-PET hypometabolism	Location of [¹¹ C]K-2 high uptake	[¹¹ C]K-2 uptake in the hippocampus	Surgery	Pathological findings	Seizure outcome (ILAE classification)
						Interictal	Ictal	Location of MRI lesion							
1	F	4	27	CBZ(400) LEV(2000) LTG(175)	1–2/M	L aT	L T	L anterior T (6)	L T (Diffuse)	L PHG	None	L ATL	HS	I	
2	M	9	53	CBZ(800) PHT(250)	1–2/W	R aT	R T	R Temporal pole and L mesial T (52)	R mesial T	R Temporal tip	None	R ATL	HS	I	
3	F	4	40	LTG(300) CBZ(400)	1–2/W	L aT	L T	L MTG and cortex facing bottom of occipitotemporal sulcus (2)	L T (Diffuse)	L PHG, FG, temporal tip	None	L ATL	HS	I	
4	F	7	58	VPA(800) ZNS(300) CBZ(200) LTG(75) DZP(15)	1–3/W	R a-mT	Non-localizable	R mesial and lateral T (32)	R T (Diffuse)	R MTG, ITG	None	R ATL	HS	I	
5	F	13	21	LCM(400)	5/M	R aT > L aT	R T	R and L T (18)	R T (Diffuse)	R Amygdala, hippocampus	High uptake	R ATL without hippocampectomy	Heterotopia	4	

AED, anti-epileptic drug; aT, anterior temporal; a-mT, anterior–middle temporal; ATL, anterior temporal lobectomy; HS, hippocampal sclerosis; IFG, inferior frontal gyrus; L, left; MTG, middle temporal gyrus; R, right; T, temporal.

Intracranial electroencephalogram

EPI-5 underwent an intracranial electrode implantation. The EEG onset for each seizure was determined as the time at which unequivocal EEG changes appeared along with the seizure onset. Ictal EEG changes that started within 500 ms from the EEG onset were defined as early ictal iEEG changes.²⁶ The region that corresponded to the electrode detecting early ictal iEEG changes was defined as the SOZ.

In vivo PET and MRI imaging

[¹¹C]K-2 was synthesized at Yokohama City University Hospital in accordance with the good manufacturing practice ordinance and was certified by the Japanese Society of Nuclear Medicine. PET imaging was performed with a Toshiba Aquiduo scanner (Toshiba Medical), which provided an axial field of view (FOV) of 240 mm and 80 contiguous 2.0-mm-thick slices. A 4.7-s transmission scan was performed for attenuation correction, and a 60-s intravenous injection of [¹¹C]K-2 (378 ± 19 MBq) was administered, followed by an emission scan of 90 min, with frames of 12×10 , 2×30 , 7×60 s, 1×2 , 1×3 , 3×5 and 6×10 min. Dynamic images were reconstructed with a 2D-ordered subset expectation maximization using four iterations, 14 subsets, a 128 matrix, a zoom of 2.8 and a 5.0-mm Gaussian filter. To permit the accurate delineation of brain regions for data analysis, each participant underwent an MRI scan on a GE SIGNA 3.0-T scanner (GE Medical Systems). Images were acquired with a proton-density-weighted sequence [time to echo = 17 ms, repetition time = 6000 ms, FOV = 22 cm (two-dimensional), matrix = 256×256 , slice thickness = 2 mm and number of excitations = 2].

PET and MRI analysis

MRI segmentation

The T₁-weighted MRI was segmented into probability maps of grey matter, white matter and CSF using the statistical parametric mapping (SPM)8 (Wellcome Department of Imaging Neuroscience). The grey matter and CSF probability maps were processed with an 8 mm full width half maximum Gaussian filter, to match the MRI spatial resolution with that of the PET scanner. The white matter areas were determined to fulfil the following conditions for voxel value: white matter probability map >0.9, smoothed grey matter map <0.05 and smoothed CSF map <0.05, according to a method described previously.¹⁶

Standardized uptake value ratio images

Since white matter is suitable as a reference region for [¹¹C]K-2-PET images, no AMPA receptor expression was detected in the white matter, as described previously,¹⁶ we obtained standardized uptake value ratio (SUVR) images using white matter as a reference region. We found that the summation image of SUVR between 30 and 50 min (SUVR_{30–50 min}) after radiotracer injection closely correlated with the AMPA

receptors density.¹⁶ Furthermore, SUVR_{30–50 min}–1 exhibited a good linear relationship with the non-displaceable binding potential [BP_{ND} ; a quantitative index of receptor density used in PET receptor imaging, quantified from the slope obtained from Logan graphical analysis (LGA) with white matter as a reference region],²⁷ which showed that SUVR_{30–50 min}–1 is an appropriate surrogate outcome for BP_{ND} .¹⁶ Based on these findings, the summation images of [¹¹C]K-2 PET during 30–50 min after radiotracer injection were obtained from patients with MTLE and co-registered to the T₁-weighted MRI. PET images and T₁-weighted MRI images were spatially normalized into Montreal Neurological Institute (MNI) standard space using SPM12. To focus on temporal lobe imagings of [¹¹C]K-2, the mask image of temporal lobe was applied, defined the following conditions for voxel value; grey matter map >0.5 and temporal lobe with Wake Forest University PickAtlas Tool. Finally, the masked PET images were transformed MNI space to native space using the inverse deformation field.

Quantitative analysis of [¹¹C]K-2 uptake

To calculate SUVR values of arrow-indicated areas and contralateral areas at temporal lobe, the volume of interests (VOIs) were manually defined on the basis of the anatomically symmetrical coordinates. The VOIs consisted of $10 \times 10 \times 10$ mm that were placed in fusiform gyrus (FG), middle temporal gyrus (MTG), hippocampus (HIP) and inferior temporal gyrus (ITG) using the PMOD Fusion tool v3.7 (PMOD Technologies). We calculated SUVR values and quantified values of the ratio of arrow-indicated areas to contralateral areas.

Data availability

All requests for raw and analysed data are promptly reviewed by the Yokohama City University Research Promotion Department to determine whether the request is subject to any intellectual property or confidentiality obligations and, further, inspected by the Institutional Review Board of Yokohama City University Hospital. Upon these approvals, derived data will be released via a material transfer agreement from the corresponding author.

Results

To examine the role of AMPARs in the genesis of epileptic discharges, we PET-scanned five patients with MTLE who underwent anterior temporal lobectomy using [¹¹C]K-2. First, we prepared the summation images of [¹¹C]K-2 over 30–50 min after the radiotracer injection and created SUVR_{30–50 min} images using white matter as a reference region, as described previously.¹⁶ In the previous study, we demonstrated that SUVR_{30–50 min} of each VOI in the resected regions of these MTLE patients with the administration of [¹¹C]K-2 represents the density of AMPARs.¹⁶ Further, LGA using white matter as a reference of these MTLE

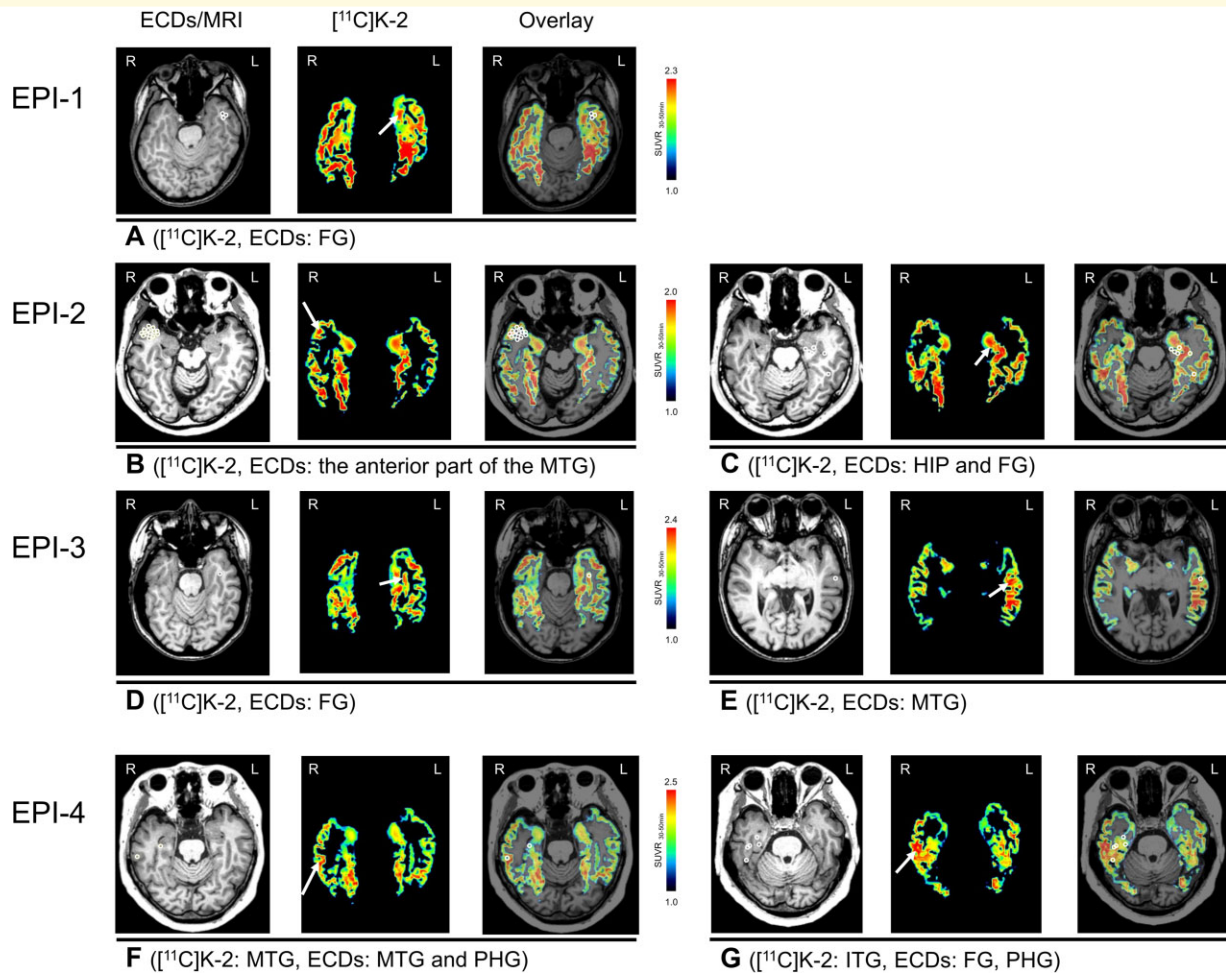


Figure 1 Increased [^{11}C]K-2 signals colocalize with ECDs in $\text{SUVR}_{30-50 \text{ min}}$ images of temporal lobes in patients with MTL.

Representative [^{11}C]K-2 $\text{SUVR}_{30-50 \text{ min}}$ images are shown restricted to temporal lobes where ECDs are estimated. Each panel shows ECDs on MRI (left), [^{11}C]K-2 (middle) and overlay (right). White arrows indicate the area showing elevated [^{11}C]K-2 uptakes and white circles indicate estimated ECDs. (A) EPI-1 showed elevated [^{11}C]K-2 uptake and estimated ECDs in the left FG. EPI-2 showed elevated [^{11}C]K-2 uptake and estimated ECDs in the anterior part of the right MTG (B) and, further, elevated [^{11}C]K-2 uptake and estimated ECDs were identified in the left HIP and the anterior part of FG. One ECD (posterior white circle) was estimated in the posterior part of FG (C). EPI-3 showed elevated [^{11}C]K-2 uptake (white arrow) and estimated ECD (white circle) in the left FG (D) and, further, elevated [^{11}C]K-2 uptake and estimated ECDs were identified in left MTG (E). EPI-4 showed elevated [^{11}C]K-2 uptake (white arrow) and estimated ECD (outer white circle) in MTG and the other ECD was estimated in the parahippocampal gyrus (PHG, inner white circle) (F). Furthermore, elevated [^{11}C]K-2 uptake was identified in the right ITG and estimated ECDs were identified in FG, adjacent closely to ITG, PHG (G).

patients with the radiotracer injection exhibited linearity of the plot, indicating reversible binding kinetics of [^{11}C]K-2 in these patients.¹⁶ From the slope of the plots obtained from LGA of these MTL patients, BP_{ND} (a quantitative index of receptor density used in PET receptor imaging) was calculated, and the good linear relationship was observed between BP_{ND} and $\text{SUVR}_{30-50 \text{ min}}$, suggesting that $\text{SUVR}_{30-50 \text{ min}}$ can be an appropriate surrogate marker for BP_{ND} .¹⁶ Thus, we used $\text{SUVR}_{30-50 \text{ min}}$ for the analysis of [^{11}C]K-2 in MTL patients described above. We also performed MEG in all five patients and iEEG in one patient (EPI-5). The locations of the ECDs that were estimated using MEG are described in Table 1, Figs 1 and 2A and B.

EPI-1 showed six ECDs in the left anterior part of the temporal lobe, five of which were estimated in the FG where we observed elevated [^{11}C]K-2 uptake, compared with the contralateral hemisphere (Fig. 1A). EPI-2 showed 52 ECDs (41 in the right and 11 in the left temporal lobe), which mostly clustered in the right temporal pole that belongs to the anterior part of the superior and middle temporal gyri. This patient also showed increased [^{11}C]K-2 uptake mainly in the right anterior part of the MTG of the temporal pole, with high colocalization of the right ECDs and increased [^{11}C]K-2 (Fig. 1B). Eleven ECDs in the left temporal lobe were estimated in the HIP and FG, most of which were colocalized with increased [^{11}C]K-2 (Fig. 1C). EPI-3 showed two

ECDs, one in the left FG that faced the bottom of the occipitotemporal sulcus and the other in the left MTG. We found increased [^{11}C]K-2 signals in these brain areas compared with the other hemispheres (Fig. 1D and E). EPI-4 showed 32 ECDs that were mostly distributed extensively

in the right temporal lobe. We found colocalization of elevated [^{11}C]K-2 uptake and ECDs in the lateral part of the right MTG (Fig. 1F). Furthermore, elevated [^{11}C]K-2 uptake was observed in the right ITG, which was adjacent closely to fusiform and parahippocampal gyrus where some ECDs

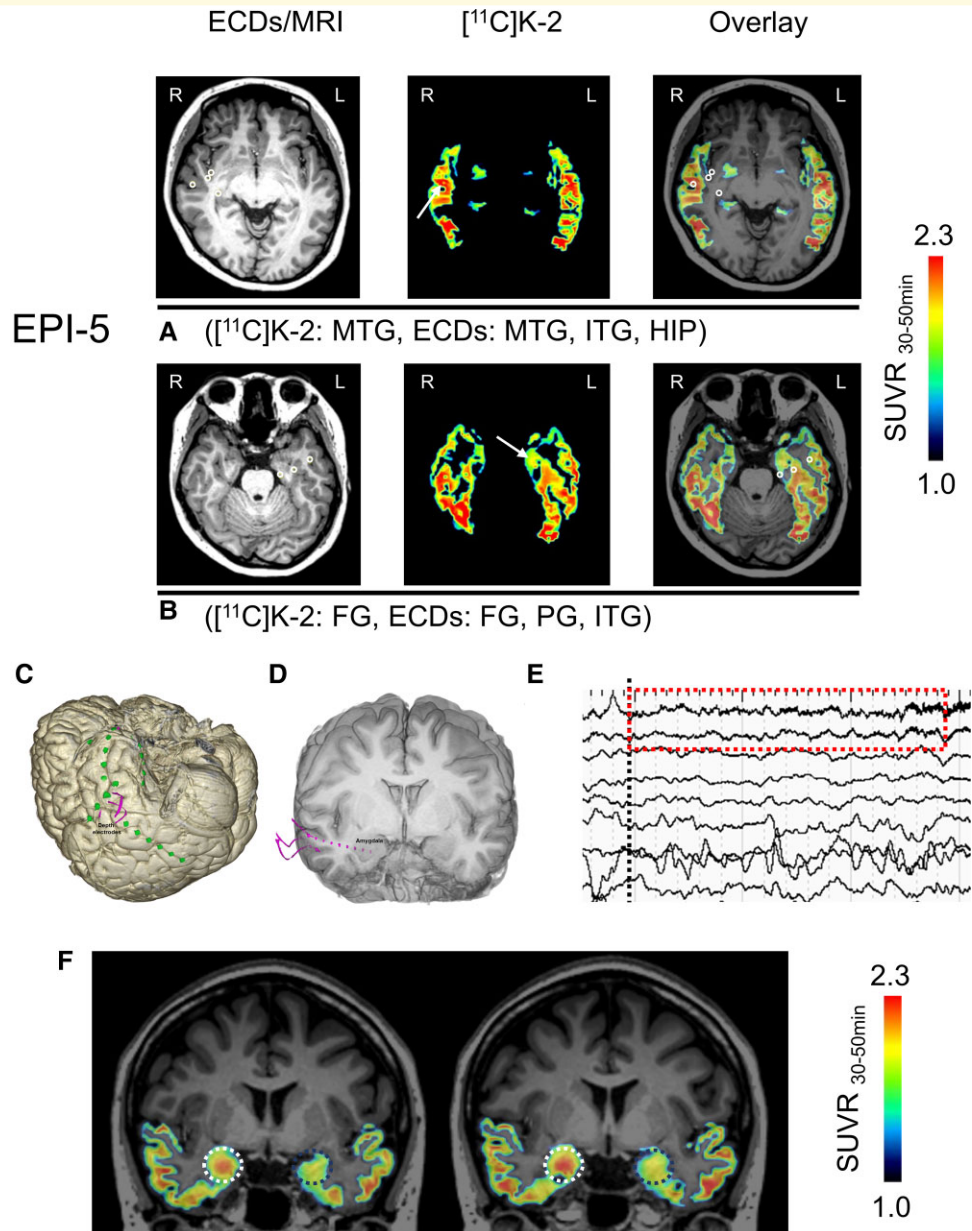


Figure 2 [^{11}C]K-2 is highly taken up in the SOZ. (A and B) Representative [^{11}C]K-2 $\text{SUVR}_{30-50\text{min}}$ images are shown, restricted to temporal lobes where ECDs are estimated. Each panel shows ECDs on MRI (left), [^{11}C]K-2 (middle) and overlay (right). White arrows indicate the area showing elevated [^{11}C]K-2 uptakes and white circles indicate estimated ECDs. EPI-5 showed elevated [^{11}C]K-2 uptake and estimated ECDs in the right MTG and, further, other ECDs were estimated in right ITG and HIP (A). Furthermore, elevated [^{11}C]K-2 uptake and estimated ECDs were identified in the left FG, and other ECDs were estimated in left PG and ITG (B). (C) The area where subdural electrodes are implanted in EPI-5. Pink lines show depth electrodes and green dots show brain surface electrodes. (D) Three depth electrodes were implanted targeting to right amygdala (pink lines and dots). (E) The iEEG change at the seizure onset (ictal EEG onset) is shown with black dots line. The earliest iEEG change (low-voltage fast activity indicated by red-dashed square) was detected by the depth electrode in right amygdala alone. The activity was the first unequivocal change at the ictal onset phase. Therefore, we deemed that the amygdala was the SOZ in this patient. (F) The zoomed image of red-dashed square in Fig. 2E shows that low-voltage fast activity occurs in the right amygdala. (G) $\text{SUVR}_{30-50\text{min}}$ images show that the elevated [^{11}C]K-2 uptake colocalizes with the SOZ (right amygdala: white dots circle). The contralateral amygdala is indicated as a dotted blue circle.

Table 2 Quantitative assessment of elevated [¹¹C]K-2 uptake

Patient	Location	Figure panel	SUVR _{30–50 min}		
			Arrow-indicated area	Contralateral area	Ratio
EPI-1	FG	Fig. 1A	2.05	1.78	15.12
EPI-2	Anterior MTG	Fig. 1B	1.83	1.64	11.22
	HIP and FG	Fig. 1C	1.81	1.76	3.30
EPI-3	FG	Fig. 1D	2.04	1.75	16.72
	MTG	Fig. 1E	2.35	2.23	5.05
EPI-4	MTG	Fig. 1F	2.40	2.04	17.56
	ITG	Fig. 1G	2.34	1.96	18.99
EPI-5	MTG	Fig. 2A	1.93	1.84	4.82
	FG	Fig. 2B	2.21	2.18	1.37
Average			2.10 ^a	1.91	10.46
SD			0.21	0.19	6.49

^aStatistical significance between SUVRs of arrow-indicated area and contralateral area ($P=0.002$, paired t -test, $n=9$).

were estimated as shown in Fig. 1G. EPI-5 showed 18 ECDs in the bilateral temporal lobes sparsely (11 in the left temporal lobe and 7 in the right temporal lobe). In this patient, the ECDs were not clearly colocalized with increased [¹¹C]K-2 signals in either temporal lobe (Fig. 2A and B). No ECDs were identified in the right amygdala, where we observed the highest [¹¹C]K-2 uptake (Fig. 2F). Prior to surgical resection, the patient was implanted with iEEG electrodes (Fig. 2C and D). At the onset of the patient's habitual seizures, low-voltage fast activities were detected on the depth electrode contacts implanted into the right amygdala (Fig. 2E and Supplementary Fig. 1), which was expected to be the SOZ, as well as increased [¹¹C]K-2 uptake (Fig. 2F). These results suggest that epileptic discharges initiated from brain areas with elevated AMPAR levels.

To clarify the significant elevated [¹¹C]K-2 uptake, we performed VOI-analysis by placing VOIs on the areas indicated by arrows in figures and VOIs on the contralateral areas to elucidate SUVR_{30–50} of each VOI (Table 2). All areas indicated by arrows in the figures had increased SUVR_{30–50} compared with those of contralateral sides with the statistical significance.

Discussion

Although a number of previous studies have suggested a relationship between increased AMPARs and epileptic activities, it has not been clearly specified whether epileptic discharges originate from brain areas with high AMPAR expression in patients with epilepsy, due to the lack of technology to visualize AMPARs in living human brains. For example, surgical specimens were reported to contain increased AMPARs, and the strict brain areas that initiate epileptic discharge should be much smaller than the areas that undergo surgical resection.^{28,29} Furthermore, although the administration of perampanel, a non-competitive AMPAR antagonist, has been effective for refractory epilepsy,¹⁵ the anti-epileptic effect of systemic AMPAR antagonists administration does not prove that brain areas with elevated AMPAR expression are responsible for the initiation of

epileptic discharges. In this study, using PET imaging with [¹¹C]K-2, we found that epileptic discharges detected by MEG or iEEG initiated from brain areas with high AMPAR expression in patients with MTLE. Since AMPAR is a principal component of excitatory glutamatergic synaptic function, this study provides a strong biological basis for the genesis of epileptic discharges.

While MEG is a powerful non-invasive modality for localizing the epileptogenic zone, it has some technological and methodological limitations. First, MEG is far less sensitive to epileptic activities that occur in deep brain areas, such as the amygdala, HIP, insula and cingulum, in which MEG could not properly localize brain areas with epileptic discharges. In contrast, PET imaging with [¹¹C]K-2 appeared to localize the SOZ in deep brain areas, as detected by iEEG. Second, MEG can miss rare and infrequent epileptic discharges due to the limited recording duration, while [¹¹C]K-2 has the potential to identify the entire epileptogenic zone by measuring AMPAR expression levels. For these reasons, the areas with high uptake of [¹¹C]K-2 are expected to be broader than the areas where ECDs are detected, leading to the mismatch of the areas indicated by [¹¹C]K-2 and MEG. Indeed, increased [¹¹C]K-2 uptakes were observed in the lateral temporal cortex especially in EPI-2 and 4. This observation does not contradict the diagnosis of MTLE, since some degree of epileptogenicity exists in the lateral temporal cortex. These two patients had the long history of epilepsy, which facilitated the establishment of the 'epileptic' neural networks to connect the mesial and lateral temporal regions.³⁰ IEDs have often been observed in the lateral temporal cortex beyond the mesial temporal structures and sometimes beyond the surgical resection areas, and these propagations were correlated with unfavourable seizure outcomes after surgery.³¹ Furthermore, the cumulative evidence indicated that the selective treatment to the HIP or to the mesial temporal structures were inferior to the anterior temporal lobectomy in terms of the chance of seizure freedom.^{32,33} The finding of the elevated uptake of [¹¹C]K-2 in the lateral temporal cortex might be useful for the prediction of treatment outcomes.

On the other hand, patients other than EPI-5 did not show increased [^{11}C]K-2 uptake in the affected HIP even though these patients had hippocampal sclerosis that has been considered to be epileptogenic zone as an aetiology of epilepsy (Table 1). As a reason for this mismatch, we expect that EPI 1–4 had reduced number of hippocampal neurons as their pathological findings, and elevated uptakes of [^{11}C]K-2 were not observed in the affected HIP even though the number of AMPA receptor in a living single neuron might be increased that could result in epileptic discharges. This expectation suggests that limited number of neurons having increased AMPA receptors is sufficient to introduce clinical seizure. It is also plausible that homeostatic plasticity reverts the expression of AMPA receptor in the affected HIP and mesial temporal cortex where the ECDs were not accompanied by the high uptake of [^{11}C]K-2 observed in EPI-2 and 4. Previous works supported this hypothesis that the increased AMPA receptors in the epileptogenic zones may gradually decrease to normal levels potentially due to the synaptic scaling.^{34–36} This hypothesis might propose the unique characteristic of [^{11}C]K-2 that could delineate the currently active regions where epileptic discharges are observed frequently and, in the other words, homeostatic plasticity has not been achieved.

Thus, PET imaging with [^{11}C]K-2 provides a powerful non-invasive tool for identifying the potential epileptogenic zone, thereby increasing diagnostic accuracy during presurgical evaluations and eventually improving surgical outcomes. Clinically, the introduction of PET imaging with [^{11}C]K-2 can dramatically change the presurgical practice of refractory epilepsy.

Ethics statement

This study was carried out as a retrospective secondary analysis using a dataset that was obtained from the clinical study; UMIN000025090 for the clinical trial with patients with epilepsy (the date of the first treatment was March 27, 2017, and that of the last treatment was January 7, 2019). The secondary analysis was performed under protocols approved by the Yokohama City University Human Investigation Committee in accordance with the ethical guidelines for medical and health research involving human subjects drawn up by the Japan Ministry of Health, Labor and Welfare. The secondary analysis protocol was registered under the number jRCTs1030210154.

Funding

This project was supported by Ministry of Education, Culture, Sports, Science and Technology (Special Coordination Funds for Promoting Science and Technology) (T.T.) and the Japan Agency for Medical Research and Development (AMED) under grant numbers JP20dm0107124 (T.T.), JP18dm0207023 (T.T.) and JP19lm0203007 (T.T.). This project was partially supported

by the Japan Society for the Promotion of Science KAKENHI under grant numbers 20H05922 (T.T.), 20H00549 (T.T.) and AMED under grant number JP21dm0207072 (T.T.).

Competing interests

T.T. and T.M. are the inventors on a patent application claiming a novel compound that specifically binds to the AMPA receptor, which includes [^{11}C]K-2. The patent used in this work is ‘Novel compound that specifically binds to AMPA receptor’ (WO/2017/006931), filed with the Shobayashi International Patent and Trademark Office.

Supplementary material

Supplementary material is available at *Brain Communications* online.

References

- Chen Z, Brodie MJ, Liew D, Kwan P. Treatment outcomes in patients with newly diagnosed epilepsy treated with established and new antiepileptic drugs: A 30-year longitudinal cohort study. *JAMA Neurol.* 2018;75:279–286.
- Rosenow F, Lüders H. Presurgical evaluation of epilepsy. *Brain.* 2001;124:1683–1700.
- Henley JM, Wilkinson KA. Synaptic AMPA receptor composition in development, plasticity and disease. *Nat Rev Neurosci.* 2016; 17:337–350.
- Huganir RL, Nicoll RA. AMPARs and synaptic plasticity: The last 25 years. *Neuron.* 2013;80(3):704–717.
- Kessels HW, Malinow R. Synaptic AMPA receptor plasticity and behavior. *Neuron.* 2009;61:340–350.
- Miyazaki T, Abe H, Uchida H, Takahashi T. Translational medicine of the glutamate AMPA receptor. *Proc Jpn Acad Ser B Phys Biol Sci.* 2021;97:1–21.
- Takahashi T, Svoboda K, Malinow R. Experience strengthening transmission by driving AMPA receptors into synapses. *Science.* 2003;299:1585–1588.
- Jitsuki S, Takemoto K, Kawasaki T, et al. Serotonin mediates cross-modal reorganization of cortical circuits. *Neuron.* 2011; 69:780–792.
- Mitsushima D, Ishihara K, Sano A, Kessels HW, Takahashi T. Contextual learning requires synaptic AMPA receptor delivery in the hippocampus. *Proc Natl Acad Sci U S A.* 2011;108:12503–12508.
- Mitsushima D, Sano A, Takahashi T. A cholinergic trigger drives learning-induced plasticity at hippocampal synapses. *Nat Commun.* 2013;4:2760.
- Takemoto K, Iwanari H, Tada H, et al. Optical inactivation of synaptic AMPA receptors erases fear memory. *Nat Biotechnol.* 2017; 35:38–47.
- Abe H, Jitsuki S, Nakajima W, et al. CRMP2-binding compound, edonepic maleate, accelerates motor function recovery from brain damage. *Science.* 2018;360:50–57.
- Zilles K, Qü MS, Köhling R, Speckmann EJ. Ionotropic glutamate and GABA receptors in human epileptic neocortical tissue: Quantitative in vitro receptor autoradiography. *Neuroscience.* 1999;94:1051–1061.
- French JA, Krauss GL, Wechsler RT, et al. Perampanel for tonic-clonic seizures in idiopathic generalized epilepsy: A randomized trial. *Neurology.* 2015;85:950–957.

15. Krauss GL, Serratosa JM, Villanueva V, *et al.* Randomized phase III study 306: Adjunctive perampanel for refractory partial-onset seizures. *Neurology*. 2012;78:1408–1415.
16. Miyazaki T, Nakajima W, Hatano M, *et al.* Visualization of AMPA receptors in living human brain with positron emission tomography. *Nat Med*. 2020;26:281–288.
17. Arisawa T, Miyazaki T, Ota W, *et al.* [11C]K-2 image with positron emission tomography represents cell surface AMPA receptors. *Neurosci Res*. 2021;173:106–113.
18. Hatano M, Miyazaki T, Ishiwata Y, *et al.* Biodistribution and radiation dosimetry of the positron emission tomography probe for AMPA receptor, [(11)C]K-2, in healthy human subjects. *Sci Rep*. 2021;11:1598.
19. Iwasaki M, Nakasato N. MEG in epilepsy and pre-surgical functional mapping. In: Supek S, Aine C, eds. *Magnetoencephalography*. Springer; 2019:1035–1058.
20. da Silva FL. EEG and MEG: Relevance to neuroscience. *Neuron*. 2013;80:1112–1128.
21. Hari R, Baillet S, Barnes G, *et al.* IFCN-endorsed practical guidelines for clinical magnetoencephalography (MEG). *Clin Neurophysiol*. 2018;129:1720–1747.
22. Iwasaki M, Nakasato N, Shamoto H, *et al.* Surgical implications of neuromagnetic spike localization in temporal lobe epilepsy. *Epilepsia*. 2002;43:415–424.
23. Kim JA, Davis KD. Magnetoencephalography: Physics, techniques, and applications in the basic and clinical neurosciences. *J Neurophysiol*. 2021;125:938–956.
24. Duez L, Tankisi H, Hansen PO, *et al.* Electromagnetic source imaging in presurgical workup of patients with epilepsy: A prospective study. *Neurology*. 2019;92:e576–e586.
25. Nissen IA, Stam CJ, Citroen J, Reijneveld JC, Hillebrand A. Preoperative evaluation using magnetoencephalography: Experience in 382 epilepsy patients. *Epilepsy Res*. 2016;124:23–33.
26. Perucca P, Dubeau F, Gotman J. Intracranial electroencephalographic seizure-onset patterns: Effect of underlying pathology. *Brain*. 2014;137:183–196.
27. Logan J, Fowler JS, Volkow ND, Wang GJ, Ding YS, Alexoff DL. Distribution volume ratios without blood sampling from graphical analysis of PET data. *J Cereb Blood Flow Metab*. 1996;16:834–840.
28. Jehi L. The epileptogenic zone: Concept and definition. *Epilepsy Curr*. 2018;18:12–16.
29. Lüders HO, Najm I, Nair D, Widdess-Walsh P, Bingman W. The epileptogenic zone: General principles. *Epileptic Disord*. 2006;8:S1–S9.
30. Fuerst D, Shah J, Kupsky WJ, *et al.* Volumetric MRI, pathological, and neuropsychological progression in hippocampal sclerosis. *Neurology*. 2001;57:184–188.
31. Mitsuhashi T, Sonoda M, Sakakura K, *et al.* Dynamic tractography-based localization of spike sources and animation of spike propagations. *Epilepsia*. 2021;62:2372–2384.
32. Josephson CB, Dykeman J, Fiest KM, *et al.* Systematic review and meta-analysis of standard vs. selective temporal lobe epilepsy surgery. *Neurology*. 2013;80:1669–1676.
33. Kohlhase K, Zöllner JP, Tandon N, Strzelczyk A, Rosenow F. Comparison of minimally invasive and traditional surgical approaches for refractory mesial temporal lobe epilepsy: A systematic review and meta-analysis of outcomes. *Epilepsia*. 2021;62:831–845.
34. Nakajima W, Jitsuki S, Sano A, Takahashi T. Sustained enhancement of lateral inhibitory circuit maintains cross modal cortical reorganization. *PLoS One*. 2016;11:e0149068.
35. Peng X, Hughes EG, Moscato EH, Parsons TD, Dalmau J, Balice-Gordon RJ. Cellular plasticity induced by anti- α -amino-3-hydroxy-5-methyl-4-isoxazolepropionic acid (AMPA) receptor encephalitis antibodies. *Ann Neurol*. 2015;77:381–398.
36. Turrigiano GG, Nelson SB. Homeostatic plasticity in the developing nervous system. *Nat Rev Neurosci*. 2004;5:97–107.